HHS Public Access

Author manuscript

J Vasc Interv Radiol. Author manuscript; available in PMC 2021 March 01.

Published in final edited form as:

J Vasc Interv Radiol. 2020 March ; 31(3): 482–491.e4. doi:10.1016/j.jvir.2019.10.015.

HIGH FREQUENCY IRREVERSIBLE ELECTROPORATION FOR TREATMENT OF PRIMARY LIVER CANCER - A PROOF OF PRINCIPAL STUDY IN CANINE HEPATOCELLULAR CARCINOMA

Brittanie R. Partridge[1,†], **Timothy J. O'Brien**[2,†], **Melvin F. Lorenzo**[2], **Sheryl L. Coutermarsh-Ott**[1], **Sabrina L. Barry**[1], **Krystina Stadler**[1], **Noelle Muro**[1], **Mitchell Meyerhoeffer**[1], **Irving C. Allen**[1], **Rafael V. Davalos**[2], **Nick G. Dervisis**[1]

[1]Virginia-Maryland College of Veterinary Medicine, Blacksburg, VA

[2]Department of Biomedical Engineering and Mechanics, Virginia Tech, Blacksburg, VA, USA, 24061

Abstract

Purpose: To determine the safety and feasibility of percutaneous high frequency irreversible electroporation (HFIRE) for primary liver cancer, and evaluate the HFIRE-induced local immune response.

Materials and Methods: HFIRE therapy was delivered percutaneously in three canine patients with resectable hepatocellular carcinoma (HCC) in the absence of intraoperative paralytics or cardiac synchronization. Pre- and post-HFIRE biopsy samples were processed with histopathology and immunohistochemistry for CD3, CD4, CD8, and CD79a. Blood was collected on days 0, 2 and 4 for complete blood count (CBC) and chemistry. Numerical models were developed to determine the treatment specific lethal thresholds for malignant canine liver tissue and healthy porcine liver tissue.

Results: HFIRE resulted in predictable ablation volumes as assessed by post-treatment CT. No detectable cardiac interference and minimal muscle contraction occurred during HFIRE. No clinically significant adverse events occurred secondary to HFIRE. Microscopically, a well-defined ablation zone surrounded by a reactive zone was evident in the majority of samples. This zone was composed primarily of maturing collagen interspersed with CD3+/CD4−/CD8− lymphocytes, in a pro-inflammatory microenvironment. The average ablation volumes for the hepatocellular carcinoma canine patients and the healthy porcine tissue were 3.89 ± 0.74 cm^3 and 1.56 ± 0.16 cm^3, respectively (p=0.03), while the average lethal thresholds were 710 ± 28.2 V/cm and 957 ± 24.4 V/cm, respectively (p=0.0004).

Corresponding Author: Nick G. Dervisis, DVM, Ph.D., Oncology, Department of Small Animal Clinical Sciences, Virginia-Maryland College of Veterinary Medicine, Blacksburg, VA, USA. 24061, dervisis@vt.edu, Telephone/Fax (540) 231 - 7666.
†These authors contributed equally to this work

Conflicts of Interest Rafael V. Davalos and Melvin F. Lorenzo all have pending and issued patents in the area of irreversible electroporation and may receive royalties.

Conclusions: HFIRE can safely and effectively be delivered percutaneously, results in a predictable ablation volume, and is associated with lymphocytic tumor infiltration. This is the first step towards using HFIRE for treatment of unresectable liver tumors.

Keywords

High Frequency Irreversible Electroporation; Immunotherapy; Hepatocellular Carcinoma

INTRODUCTION

HCC is also common in canines, of which about 60% are surgically resectable. As in humans, non-resectable tumors carry a grave prognosis due to limited effective alternative treatment options [1], [2]. Since canine HCC appears to share many similarities in clinical behavior with HCC in humans, it could service as a model for investigation into novel therapies. More importantly, resectable canine HCC would provide the opportunity to evaluate the effectiveness of local ablative therapy prior to use in non-resectable tumors.

The liver is of particular interest because it is an immunologically rich but tolerogenic environment [3]. Thus, local ablative treatment within the liver may be able to activate the immune system, resulting in local and systemic anti-tumor immune responses. Energy-based focal ablation therapies provide an alternative to surgical resection or radiotherapy. Unlike thermal ablation therapies (radiofrequency, microwave, and cryo ablation therapies), IRE relies on the administration of short, intense, pulsed electric fields to induce non-thermal irrevocable disruption of homeostasis and cell death [4], [5]. Consequently, this therapy encourages a unique immune response compared to other ablative techniques. More recently, it was shown that IRE could trigger as much as 2 – 3 times the amount of T cell proliferation in comparison to thermal therapies [6]. Despite this exciting revelation, required cardiac synchronization and intraoperative paralytics can make IRE procedures somewhat cumbersome [7], [8].

High-frequency irreversible electroporation (HFIRE) could be used to capitalize on these proinflammatory conditions post therapy, and minimize the difficulties associated with typical IRE procedures. This next generation of IRE negates the need for cardiac synchronization and paralytics by using rapid bipolar pulses that minimize nerve and muscle excitation [9–12]. Further, HFIRE therapy has been shown to preferentially target malignant cells *in vitro* [13], [14].

The objective of this first-in-canine patient pilot study was to determine the feasibility of percutaneous HFIRE for treatment of primary liver cancer, and evaluate the immunologic response to the ablation.

MATERIALS AND METHODS

Canine Patients

Client owned canines diagnosed with HCC were recruited at the Virginia-Maryland College of Veterinary Medicine Teaching Hospital from January 2018 to March 2018. All canines were screened for inclusion with a complete blood count (CBC), serum chemistry,

urinalysis, prothrombin time, partial thromboplastin time, computed tomography (CT) imaging of the thorax and abdomen with triple phase contrast enhancement and ultrasound-guided needle core biopsy of the liver mass prior to enrollment. Inclusion criteria included the presence of a surgically resectable primary liver tumor, a histologic diagnosis of HCC, and liver enzymes less than 4X the upper reference limit. Canines were excluded if their tumor was non-resectable based on consultation with a board-certified surgeon or if survival was expected to be less than 6 weeks due to the presence of significant comorbidities. An owner informed consent was obtained before enrollment, and the study was approved by the Virginia Tech institutional animal care and use committee.

Canine Characteristics

Three canines met the inclusion criteria and were enrolled in the study. All canine patients were between 13 and 15 years old and considered geriatric [15].

Canine 1 was a 15-year-old male castrated toy poodle with concurrent diabetes mellitus (controlled), hyperadrenocorticism (untreated) and seizures (controlled) that initially presented for general malaise and subsequent bloodwork revealed elevated liver enzymes. A magnetic resonance imaging (MRI) performed after initial diagnosis of HCC revealed a small primary brain tumor in the left frontal lobe most consistent with a meningioma and probable small cerebral hemorrhages.

Canine 2 was a 13-year-old female spayed mixed breed dog with concurrent hypothyroidism (medically controlled) that was asymptomatic on presentation but routine bloodwork revealed significant increases in liver enzymes, which initiated a thorough work-up.

Canine 3 was a 14-year-old male castrated toy poodle with no significant concurrent medical conditions that presented with clinical signs of anorexia and weight loss.

Imaging

All canines were imaged using a Toshiba Aquilion CT scanner and were anesthetized via inhalation anesthesia, breath hold during the scan. Precontrast, immediate, 1-minute delay and 3-minute delay scans of the thorax and abdomen were obtained using iopromide contrast agent (Ultravist, Bayer HealthCare Pharmaceuticals) and a pressure injector (Stellant, Medrad). Images were analyzed in Horos image station. Canines were imaged pre-HFIRE treatment, and 4 days post treatment.

HFIRE Treatment

A custom built HFIRE generator (EPULSUS®-FBM1–5, Energy Pulse Systems, Lisbon, Portugal) capable of producing sub-microsecond, bipolar pulses in rapid bursts was used to deliver HFIRE therapy via a single, 18-gauge bipolar electrode (AngioDynamics Inc., Latham, NY, USA) percutaneously. The generator was set to deliver 300 bursts of a voltage amplitude of 2250 V via a voltage waveform presenting pulse widths 2 μs with a 5 μs delay between each change in polarity (2-5-2; on-off-on [μs]) for a total on-time (energized-time) of 100 μs for each burst. An oscilloscope (DPO2002B, Tektronix Inc., Beaverton, OR, USA) was used to monitor the voltage and current waveforms subsequent of the signal being

attenuated using a 1000x high voltage probe (P5210A, Tektronix Inc., Beaverton, OR, USA) and passing through a current probe (2877, Pearson Electronics, Palo Alto, CA, USA). Figure 1 illustrates the bipolar electrode, a schematic of the experimental set-up, and a comparison between a typical IRE voltage waveform and the HFIRE voltage waveform utilized within this study.

HFIRE was delivered with the canines under inhalation general anesthesia in the absence of intraoperative paralytics and cardiac synchronization. However, canines were monitored continuously with electrocardiogram to visualize any potential abnormalities. Each canine was placed on dorsal recumbency, the ventral abdomen hair were clipped with surgical clippers, and surgical aseptic technique was used to advance the sterilized percutaneous HFIRE probe under ultrasonographic guidance. The ultrasonographic monitoring continued during the HFIRE treatment.

Numerical Modeling

HFIRE treatment protocol was designed to ablate a portion of the tumor tissue and elicit an immune response. Thus, numerical modeling was employed to predict electric field distributions and determine pulsing parameters that result in ablation volumes constrained to portion of the tumor tissue. Accordingly, abdominal CT images from HCC canine patients were imported into 3D Slicer (an open source platform for medical image informatics), where relevant anatomical features (liver, hepatic artery, and tumor) were segmented. Then a surface model maker tool was employed to re-construct the identified features in 3-dimensions. Each relevant geometry was transferred to 3-matic (Materialse, Leuven, Belgium), where the bipolar electrode was reconstructed and placed into the simulated tumor-tissue model. The entire assembly was meshed for import into a commercial finite element package (COMSOL Multiphysics, v.5.4; Stockholm, Sweden) for analysis.

Dynamic electrical properties were then assigned to normal and malignant tissue within patient-specific hepatic geometries using tissue data normalized to hepatic tissue properties [16]. The methods for predicting electric field distributions for HFIRE are similar to those described for IRE therapies [17–20]. The electric field distribution can be derived from equation 1 and applying the electroquasistatic approximation:

$$\nabla \cdot (\sigma \nabla \Phi) = 0 \tag{1}$$

where σ is the tissue conductivity and Φ is the electric potential. The electrical boundary conditions at the tissue-electrode interface were set to Φ = V (source) and Φ = 0 (sink). Boundaries not in contact with an electrode were treated as electrically insulating.

Applying methods adapted from O'Brien et al. [21], electrical current measured during therapy were utilized to establish treatment specific conductivity curves. Then, the minimum electric field required to induce cell death (the lethal threshold) was determined by comparing the measured volumetric ablation dimensions with those predicted from the numerical model. The electric field that corresponded to the closest matching volumetric dimensions was designated as the lethal threshold.

Siddiqui et al. [10] performed an equivalent HFIRE pulsing protocol to healthy porcine liver tissue within their study. Thus, electrical current and lesion volume data from these studies were employed, facilitating a treatment specific comparison of lethal thresholds for healthy and malignant tissue. Figure 2 illustrates each step of the 3D reconstruction process for the patient specific model, as well as a comparison between diseased and healthy hepatic tissue electric field thresholds. Details on the numerical modeling are accessible in the Supplemental Text in conjunction with the material properties applied (Supplemental Table E1).

Canine Patient Hospitalization and Tumor Resection

All canines were hospitalized post HFIRE therapy in the Intensive Care Unit (ICU) for monitoring, until surgical resection of their HCC. The surgery was performed 4 days post HFIRE treatment, immediately after the second CT scan. Tumor resection was performed using standard surgical technique. After surgery, the tumor was submitted for histopathology and immunohistochemistry. Canines were recovered in the ICU and discharged to their owners 2 days later. Recheck exam and blood collection were performed 2 weeks after surgical removal (day 14). CBC, and serum chemistry analyses were performed on blood collected at each time point.

Histopathology and Immunohistochemistry

Pre-HFIRE therapy needle core biopsies and post-HFIRE resected tumor samples were processed within 20 minutes of excision. Resected tumor sections were evaluated by a board-certified pathologist (SLC) to confirm a definitive diagnosis and assess completeness of excision. Post-HFIRE samples were grossly examined to identify regions of electroporation, non-treated tumor, and normal, non-neoplastic liver. Foci of electroporation were grossly identified in the majority of samples as well-demarcated foci of hemorrhage and necrosis. Sections were taken through these areas for examination of the treated/un-treated interface. Sections were routinely processed and stained with hematoxylin and eosin (H&E). Immunohistochemistry for CD3 (Agilent Dako, A0452, rabbit polyclonal, Anti-human), CD4 (Novus Biologicals, NBP1–19371, rabbit polyclonal, Anti-human), CD8 (Abcam, ab4055, Rabbit polyclonal, Anti-human) and CD79a (Biocare Medical, CM 067 A, C, mouse monoclonal, Anti-human) was performed to evaluate the local immune response to treatment. All antibodies were validated and run on a Ventana Benchmark XP automated stainer using the Discovery Universal secondary antibody (Roche, 760–4205), ultraView Universal Alkaline Phosphatase Red Detection Kit, and hematoxylin counterstain. All antibodies were verified to work in canine tissue prior to use in research samples (Supplemental Figure E1). Lymphocytic infiltration was subjectively quantified for comparison between pre- and post-treatment tumor samples.

Gene Expression Analysis

Formalin-fixed paraffin embedded (FFPE) pre- and post-HFIRE treatment tumor tissue was used in a super array to compare specific gene expression between pre-treatment and post-treatment. A custom, canine specific, super array developed and validated in-house was used, based on the Qiagen RT2 profiler platform. The array design contains 89 genes associated with inflammation and cancer (Supplemental Table E2), three positive controls

(actin, HPRT1, GAPDH), a genomic DNA control, a no-template control, a no-RT control, and a no-amplification control. Sections of the pretreated tumor and of the transition zone, at the ablated / non-ablated tumor of the post-treatment tumor were selected for RNA extraction. Total RNA was extracted from 10um thick slices of each of pre-treatment tumor biopsies, and post-treatment FFPE tissues. RNA extraction was performed using a Zymo kit, according to manufacturer's directions. Gene expression on each array was evaluated following the manufacture's standard protocols. Briefly, the extracted RNA was quantified and assessed through standard QA/QC. The resulting RNA samples went through 1st strand synthesis and qPCR amplification in an ABdI 7500 FAST thermocycler, according to the Qiagen RT2 profiler protocol. The RT-qPCR data were analyzed using the common Delta-Delta Ct methodology. The pre-treatment gene expression profile was compared to the post-treatment groups samples, with archived formalin fixed paraffin embedded normal liver tissue from 12 young canine patients of various breeds with congenital portosystemic shunts used for selecting housekeeping genes. Normal liver tissue was collected at the time of surgical correction. The super array results were analyzed using Qiagen's GeneGlobe Data Analysis software suite for individual gene expression differences and Ingenuity's pathway analysis (IPA) software for pathway analysis. More specifically, Ct values were exported and uploaded to a data analysis web portal (http://www.qiagen.com/geneglobe). Samples were assigned to controls and test groups. Ct values were normalized based on manual selection of reference genes that demonstrated small changes in gene expression (Ct value differences less than 1). The data analysis web portal calculates fold change/regulation using delta-delta Ct method, in which delta Ct is calculated between gene of interest (GOI) and an average of housekeeping genes (HKG), followed by delta-delta Ct calculations. Fold Change is then calculated using 2^ (−1*delta-delta Ct) formula. All data were ranked and evaluated based on z-score as previously described [22].

Statistical Analysis

A total of 3 canine patients with HCC were treated, with 1 treatment performed per patient (total N = 3). Further, a total of 3 healthy porcine were treated, with 1 treatment performed per porcine (total N=3). Data for each are presented as mean values ± standard deviation of the mean. A two-tailed student t-test was performed to determine if the ablation volumes and/or electric field thresholds were significantly different from each other. All statistical analysis was performed within JMP® Pro version 14.0.0 (SAS Institute Inc., Cary, NC).

RESULTS

Ablation Volumes and Numerically Determined Lethal Thresholds

CT Images taken from pre-HFIRE treatment and 4 days post treatment indicated an average ablation volume of 3.89 ± 0.74 cm^3. In comparison, the average ablation volume for healthy porcine tissue was 1.56± 0.16 cm^3 (Figure 2E, n=3 for both treatment groups, p=0.03) [10, 16]. The average lethal thresholds for the HCC canine tissue and the healthy porcine tissue were 710 ± 28.2 V/cm and 957 ± 24.4 V/cm, respectively (Figure 2F, n=3 for both treatment groups, p=0.0004). These results are in agreement with previous findings that suggest HFIRE therapy may preferentially target malignant cells [13]. However, more studies would

be required to make any robust conclusions about HFIRE therapies preferentially targeting malignant cells.

Feasibility and Safety of HFIRE Ablation

No clinically significant adverse events were associated with HFIRE treatment. No detectable cardiac interference occurred during HFIRE delivery and only minimal muscle contraction was noted in the absence of paralytics (Supplemental Videos E1 *and* E2). HFIRE resulted in an ablation volume visible as predicted by the numerical modeling, on CT prior to surgical resection (day 4) and in gross tumor samples following tumor excision in all three canines. Histopathology revealed a well-defined ablation/tumor interface following HFIRE in two canines and poorly defined ablation/tumor interface in a single canine (Figure 4).

Hepatotoxicity Assessment

ALT and ALP both increased compared to baseline following HFIRE treatment (day 0) but resolved over time following tumor removal on day 4 (Figure 5). These enzyme elevations were most severe in canine three at all time points. No other liver associated enzymes or hepatobilliary markers were elevated over baseline and no clinical signs associated with the HFIRE treatment were noted during the canine's hospitalization in ICU. Canine 1 was euthanized 8 days after surgery due to uncontrolled seizures attributed to the animal's brain lesions, thus recheck liver values were not available. Canines 2 and 3 are currently alive (>12 calendar months later) and undergo chest x-rays and an abdominal ultrasound every 3 months for re-staging. Neither recurrence nor metastasis has been identified in either canine to date (>12 calendar months prost treatment).

Immunologic Reaction to the Ablation

Immunohistochemistry on the tumor/ablation interface revealed subjectively increased infiltration with CD3+ lymphocytes following HFIRE treatment in two canines (Figure 3), when compared to pretreatment samples. Supplemental Figure E2 provides a visual comparison of the CD3+ infiltration pre- and post-treatment. Post-treatment samples were negative for both CD4 and CD8 positive cells, suggesting the infiltrating T-cell had a unique CD3+/CD4−/CD8− phenotype (Figure 4). CD3+ lymphocyte infiltration was absent in the canine with a poorly defined ablation/tumor interface (Figure 3). In all canines, the tumor/ablation interface was negative for CD79a+ lymphocytes.

Gene expression analysis indicated up-regulation of 21 genes associated with inflammation and activation of the innate and adaptive immune system following HFIRE treatment in all three canines. In contrast, gene expression of 29 genes associated with modulation and regulation of the immune system was downregulated following HFIRE treatment in all three canines compared to baseline. Table 1 presents the details for these findings. Further, pathway analysis indicated a specific proinflammatory signaling microenvironment in canine 1 and 2, which corresponds with the CD3+ cell infiltrations, whereas canine 3 lacks this microenviromental niche (Figure 6A – C). IPA network analysis identified two functional networks that fit the canonical pathways identified above, cell injury/death and cell mediated immunity (Figure 6D, E). Both of these networks were significantly upregulated in all canines following HFIRE treatment. However, it should be noted that

canine 3's data within the networks was actually a significant downregulation moving towards lesser downregulation. Figure 6F shows that NF-κB signaling was one of the most dominate pathways impacted by HFIRE treatment. Gene expression patterns revealed a significant global up-regulation in NF-κB signaling.

DISCUSSION

This proof of principal study was designed to determine if HFIRE therapy, delivered percutaneously, could produce rapid, predictable ablations in the absence of intraoperative paralytics and cardiac synchronization within a spontaneous canine liver tumor model. A treat and resect procedure was established to minimize any risk to the treated animals, while also permitting a thorough evaluation of the ablated tissues and the loco-regional microenvironment via removal of the entire tumor post therapy.

Energy-directed, minimally invasive procedures have been shown to activate an immune response to enhance cancer cell destruction. Recent *in vitro* studies have shown that IRE to be more influential in comparison to thermal therapies [6]. However, the requirement of intraoperative paralytics and cardiac synchronization for all IRE procedures can be an impediment, adding more complication to the modality [7], [8]. Though, HFIRE therapy, a next generation of IRE therapy, can be safely applied in the absence of intraoperative paralytics and cardiac synchronization required during traditional IRE [12], [23]. Additionally, IRE and HFIRE therapies alike can, at times, benefit from a multi-electrode (≥ 2 electrodes) configurations when attempting to encompass a large or irregularly shaped tumor. The precise placement and alignment of the electrodes to ensure the intended treatment conditions can be technically challenging and time consuming. However, the single needle, bipolar treatment probe can alleviate these concerns and provide additional advantages, including percutaneous treatment delivery.

Throughout this study, percutaneous HFIRE therapy was delivered in the absence of intraoperative paralytics and cardiac sync, resulting in predictable ablation volumes without any discernable muscle twitch or effect to cardiac function for all three canine patients. Consistent with previous findings [10], [21], these results indicate the potential of a more precise treatment plan prior to ablation of entire tumors.

The immunological reaction analysis provided a unique CD3+/CD4−/CD8− phenotype of lymphocytes infiltrating the ablation/tumor interface. This was somewhat unexpected as terminally differentiated T-cells typically express either CD4 or CD8. Double negative T-lymphocytes appear to be involved in immune regulation and tolerance, as well as host defense and inflammation [24–26]. Since the liver is an immunologically rich but active organ, the presence of these cells may serve to a role in tumor antigen recognition in response to the neoplastic cell death post HFIRE. However, canine 3 did not present a clear reactive zone histologically. Further, there was minimal lymphocytic infiltration, and the microenvironment as assessed via the super array was distinct when compared to the other two canines. Despite the abundant necrosis contained within this canines's tumor, adaptive immune cell infiltration was not detected. Additionally, due to the amount of necrosis associated with this tumor, it was difficult to appreciate the ablation zone grossly, thus it is

possible that sections submitted for histopathology did not represent the ablation/tumor interface.

A hepatotoxicity assessment indicated that liver enzymes (ALT and ALP) increased above baseline in all canines following HFIRE treatment and resolved following tumor removal. This increase was anticipated since tumor cells and normal hepatocytes likely contain similar enzymes that are released upon cell death. Canine 3 had the most severe liver enzyme elevations and took the longest for these elevations to resolve, likely secondary to the relative increased in tumor size compared to canines 1 and 2.

A unique transition zone surrounding the tumor-ablated volume was observed within 2/3 of the treated canine patients. This transition zone was characterized by a specific T-cell infiltration in a tumor microenvironment of proinflammatory signaling. This response to HFIRE may indicate a unique HFIRE / immune interaction, potentially specific to the liver neoplastic niche. Again, Canine 3 lacked both the transition zone and the proinflammatory response to HFIRE ablation, which could represent a biological variant to this ablation technique, or an inability of the technique to induce such a response to relatively more necrotic tumor.

The treatment specific numerical modeling provided lethal thresholds estimates for malignant canine and healthy porcine liver tissue. These preliminary outcomes suggest a preferential targeting of malignant cells when applying HFIRE therapy, but more work is required prior to making any full-bodied conclusions.

A major limitation of this study was its small sample size (n = 3), however, this study was designed to be a proof of principal study assessing the safety and feasibility of HFIRE therapy. Comparison of lymphocytic infiltration between pre- and post-treatment tumor samples was subjective, thus statistical significance could not be determined. Additionally, multiplexed IHC was not performed on tumor samples, thus the conclusion that infiltrating CD3+ cells are also negative for CD4 and CD8 cannot be made. Another limitation is the presence of background staining occurring in the CD4 and CD8 samples. CD4 and CD8 cross-react with dead tissue, thus the ablation zone was heavily stained in most samples, further complicating interpretation. Flow cytometry on cells isolated from the ablation/tumor interface may confirm the phenotype of infiltrating cells is currently underway.

HFIRE therapy can be safely delivered percutaneously with a predictable ablation volume. This minimally invasive ablative procedure may be associated with unique lymphocytic tumor infiltration (CD3+/CD4−/CD8−), and further, may potentially elicit preferential therapeutic targeting towards malignant cell types.

Supplementary Material

Refer to Web version on PubMed Central for supplementary material.

Acknowledgments

Source of Funding Veterinary Memorial Fund, ICTAS Center for Engineered Health, Pancreatic Cancer Action Network (PanCAN) Grant PanCAN 16-65-IANN, and the Grayton Friedlander Memorial Fund. We would like to

thank members of the VTH Oncology service (Klahn, Olsen and Wyne), VTH Radiology service (Stadler), VTH Surgery service (Muro), VTH Anesthesia (Carpenter), Dr. Coy Allen's lab (Ringel-Scala and Brock), Dr. John Rossmeisl's Lab (Arena), and Anne Avery at CSU's Clinical Immunology Lab for all of their contributions to this project.

ABBREVIATIONS:

HFIRE	high frequency irreversible electroporation
IRE	irreversible electroporation
HCC	hepatocellular carcinoma
CT	computed tomography
FFPE	formalin-fixed paraffin embedded
CBC	complete blood count
H&E	hematoxylin and eosin
ALT	alanine aminotransferase
ALP	and alkaline phosphate
IPA	ingenuity pathway analysis

REFERENCES

[1]. Balogh J, Iii DV, Gordon S, Li X, Ghobrial RM, and Jr HPM, "Hepatocellular carcinoma: a review," J Hepatocell Carcinoma, vol. 3, pp. 41–53, 2016. [PubMed: 27785449]

[2]. Liptak JM et al., "Liptak JAVMA 2004 hepatocellular carcinoma 48 dogs," vol. 225, no. 8, 2004.

[3]. Robinson MW, Harmon C, and O'Farrelly C, "Liver immunology and its role in inflammation and homeostasis," Cell. Mol. Immunol, vol. 13, no. 3, pp. 267–276, 2016. [PubMed: 27063467]

[4]. Davalos RV, Mir LM, and Rubinsky B, "Tissue ablation with irreversible electroporation," Ann. Biomed. Eng, vol. 33, no. 2, pp. 223–231, 2005. [PubMed: 15771276]

[5]. Edd JF, Horowitz L, Davalos RV, Mir LM, and Rubinsky B, "In vivo results of a new focal tissue ablation technique: Irreversible electroporation," IEEE Trans. Biomed. Eng, vol. 53, no. 7, pp. 1409–1415, 2006. [PubMed: 16830945]

[6]. Shao Q et al., "Engineering T cell response to cancer antigens by choice of focal therapeutic conditions," Int. J. Hyperth, vol. 0, no. 0, pp. 1–9, 2019.

[7]. Ball C, Thomson KR, and Kavnoudias H, "Irreversible electroporation: A new challenge in 'out of operating theater' anesthesia," Anesth. Analg, vol. 110, no. 5, pp. 1305–1309, 2010. [PubMed: 20142349]

[8]. Nielsen K et al., "Anaesthetic management during open and percutaneous irreversible electroporation," Br. J. Anaesth, vol. 113, no. 6, pp. 985–992, 2014. [PubMed: 25173767]

[9]. Arena CB et al., "High-frequency irreversible electroporation (H-FIRE) for non-thermal ablation without muscle contraction High-frequency irreversible electroporation (H-FIRE) for non-thermal ablation without muscle contraction," Biomed. Eng. Online, vol. 10, no. 1, p. 102, 2011. [PubMed: 22104372]

[10]. Siddiqui IA et al., "Induction of rapid, reproducible hepatic ablations using next-generation, high frequency irreversible electroporation (H-FIRE) in vivo," Hpb, vol. 18, no. 9, pp. 726–734, 2016. [PubMed: 27593589]

[11]. Miklovic T, Latouche EL, DeWitt MR, Davalos RV, and Sano MB, "A Comprehensive Characterization of Parameters Affecting High-Frequency Irreversible Electroporation Lesions," Ann. Biomed. Eng, vol. 45, no. 11, pp. 2524–2534, 2017. [PubMed: 28721494]

[12]. Sano MB et al., "Reduction of Muscle Contractions during Irreversible Electroporation Therapy Using High-Frequency Bursts of Alternating Polarity Pulses: A Laboratory Investigation in an Ex Vivo Swine Model," J. Vasc. Interv. Radiol, vol. 29, no. 6, pp. 893–898.e4, 6 2018. [PubMed: 29628296]

[13]. Ivey JW, Latouche EL, Sano MB, Rossmeisl JH, Davalos RV, and Verbridge SS, "Targeted cellular ablation based on the morphology of malignant cells," Sci. Rep, vol. 5, pp. 1–17, 2015.

[14]. Ivey JW, Bonakdar M, Kanitkar A, Davalos RV, and Verbridge SS, "Improving cancer therapies by targeting the physical and chemical hallmarks of the tumor microenvironment," Cancer Lett, vol. 380, no. 1, pp. 330–339, 2016. [PubMed: 26724680]

[15]. Moore AS and Frimberg AE, "Usefulness of chemotherapy for the treatment of very elderly dogs with multicentric lymphoma," JAMA, vol. 252, no. 7, 2018.

[16]. Hasgall P et al., "IT'IS Database for thermal and electromagnetic parameters of biological tissues," vol. Version 4, 2018.

[17]. Edd JF and Davalos RV, "Mathematical Modeling of Irreversible Electroporation for Treatment Planning," Technol. Cancer Res. Treat, vol. 6, no. 4, pp. 275–286, 2007. [PubMed: 17668934]

[18]. Garcia PA et al., "Non-Thermal Irreversible Electroporation (N-TIRE) and Adjuvant Fractionated Radiotherapeutic Multimodal Therapy for Intracranial Malignant Glioma in a Canine Patient," Technol. Cancer Res. Treat, vol. 10, no. 1, pp. 73–83, 2011. [PubMed: 21214290]

[19]. Garcia PA, Rossmeisl JH, Neal RE, Ellis TL, and Davalos RV, "A parametric study delineating irreversible electroporation from thermal damage based on a minimally invasive intracranial procedure," Biomed. Eng. Online, vol. 10, no. 4, 2011.

[20]. Latouche EL, Sano MB, Lorenzo MF, Davalos RV, and Martin RCG, "Irreversible electroporation for the ablation of pancreatic malignancies: A patient-specific methodology," J. Surg. Oncol, vol. 115, no. 6, pp. 711–717, 2017. [PubMed: 28185295]

[21]. O'Brien TJ et al., "Experimental High-Frequency Irreversible Electroporation Using a Single-Needle Delivery Approach for Nonthermal Pancreatic Ablation In Vivo," J. Vasc. Interv. Radiol, vol. 30, no. 6, pp. 854–862.e7, 6 2019. [PubMed: 31126597]

[22]. Ringel-Scaia VM et al., "High-frequency irreversible electroporation is an effective tumor ablation strategy that induces immunologic cell death and promotes systemic anti-tumor immunity," EBioMedicine, vol. 44, p. 112–125, 6 2019. [PubMed: 31130474]

[23]. Arena CB et al., "High-frequency irreversible electroporation (H-FIRE) for non-thermal ablation without muscle contraction," Biomed. Eng. Online, vol. 10, no. 1, p. 102, 2011. [PubMed: 22104372]

[24]. Martina MN, Noel S, Saxena A, Rabb H, and Hamad ARA, "Double negative (DN) αβ T cells: misperception and overdue recognition," Immunol. Cell Biol, vol. 93, no. 3, pp. 305–310, 3 2015. [PubMed: 25420721]

[25]. D'Acquisto F and Crompton T, "CD3+CD4−CD8− (double negative) T cells: Saviours or villains of the immune response?," Biochem. Pharmacol, vol. 82, no. 4, pp. 333–340, 2011. [PubMed: 21640713]

[26]. Ford MS, Young KJ, Zhang Z, Ohashi PS, and Zhang L, "The immune regulatory function of lymphoproliferative double negative T cells in vitro and in vivo," J. Exp. Med, vol. 196, no. 2, pp. 261–267, 7 2002. [PubMed: 12119351]

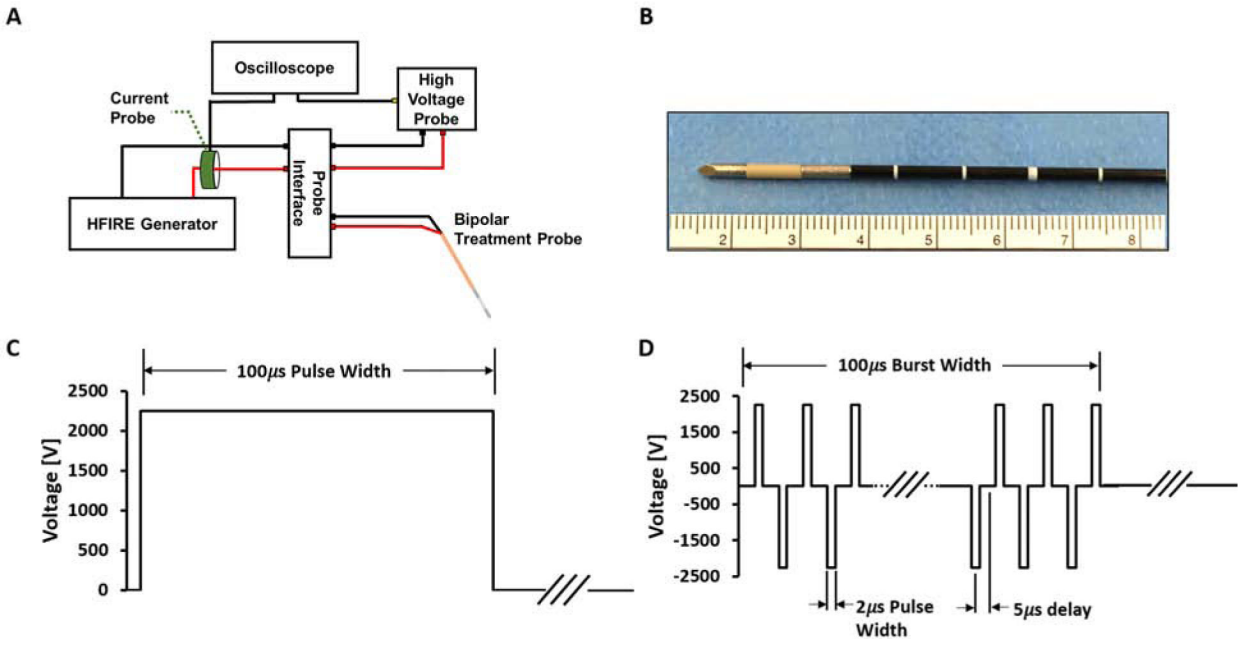

Figure 1.

(A) Schematic of HFIRE experimental set-up and **(B)** 18-gauge, bipolar electrode. **(C)** A standard IRE voltage waveform pulse and **(D)** a representative HFIRE voltage waveform (2-5-2 (on-off-on [μs])). Twenty-five bipolar pulses contribute to a single HFIRE burst with a burst width of 100 μs.

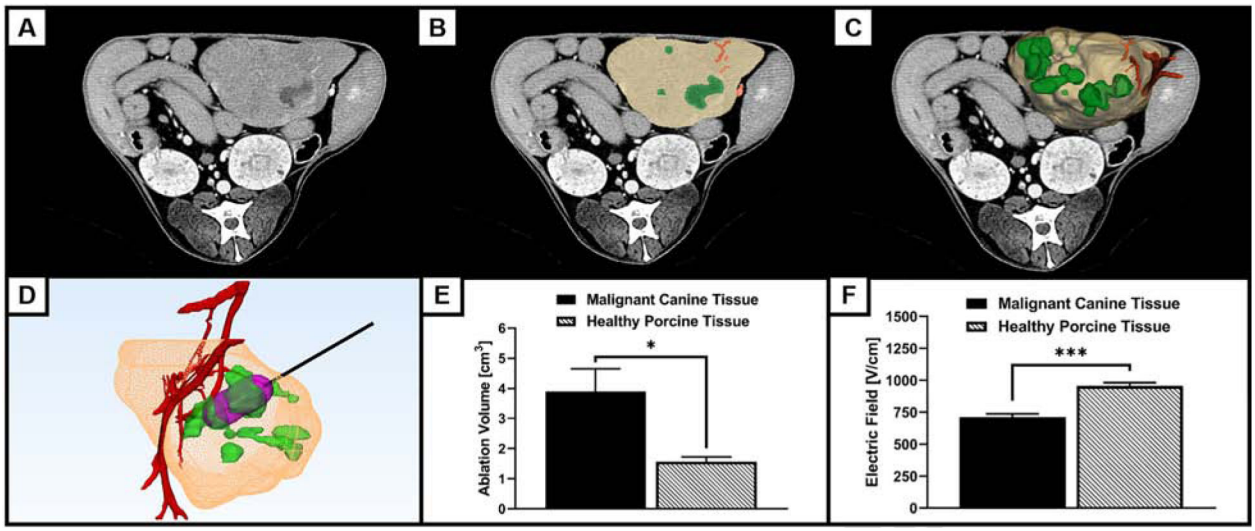

Figure 2.

(A) Schematic of the 3D-reconstruction and numerical modeling process for canine 1. CT images were imported into 3D slicer **(A)**, where the relevant features were highlighted on each CT image **(B)**. Then a surface maker was utilized to interpolate between each slice and reconstruct the identified features in 3-dimensions **(C)**. All relevant features were transferred to 3-matic for assembly with the bipolar electrode and meshing for analysis within COMSOL v5.4 **(D)**. **(E)** The average ablation volumes for the malignant canine patients and the healthy porcine tissue were 3.89 ± 0.74 cm^3 and 1.56 ± 0.16 cm^3, respectively (p=0.03). **(F)** The average lethal thresholds were 710 ± 28.2 V/cm and 957 ± 24.4 V/cm, respectively (p=0.0004).

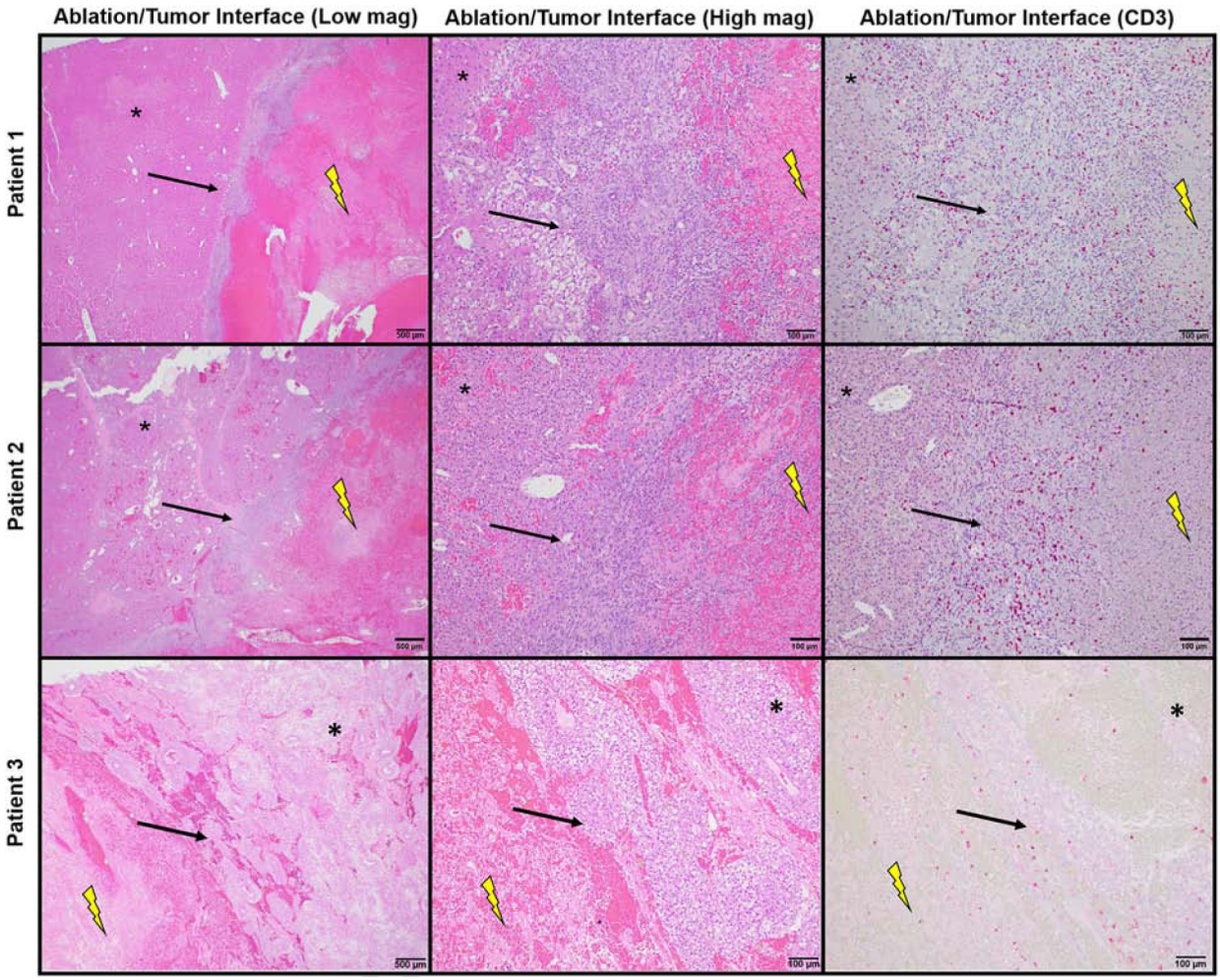

Figure 3.

Tumor histopathology from canine 1 (top) and canine 2 (middle) showing the well-defined ablation/tumor interface (arrows) with H&E at 40X (left) and 100X (center). Immunohistochemistry for CD3 revealed positive (red) staining cells infiltrating the tumor-ablation interface. Canine 3 (bottom) showing absence of a well-defined ablation/tumor interface (arrows) with H&E at 40X (left) and 100x (center). Immunohistochemistry for CD3 (right) shows the lack of CD3+ cells within the ablation/tumor interface. Positively stained cells are red. Untreated HCC is denoted by (*) and the ablation tumor volume by the bolt.

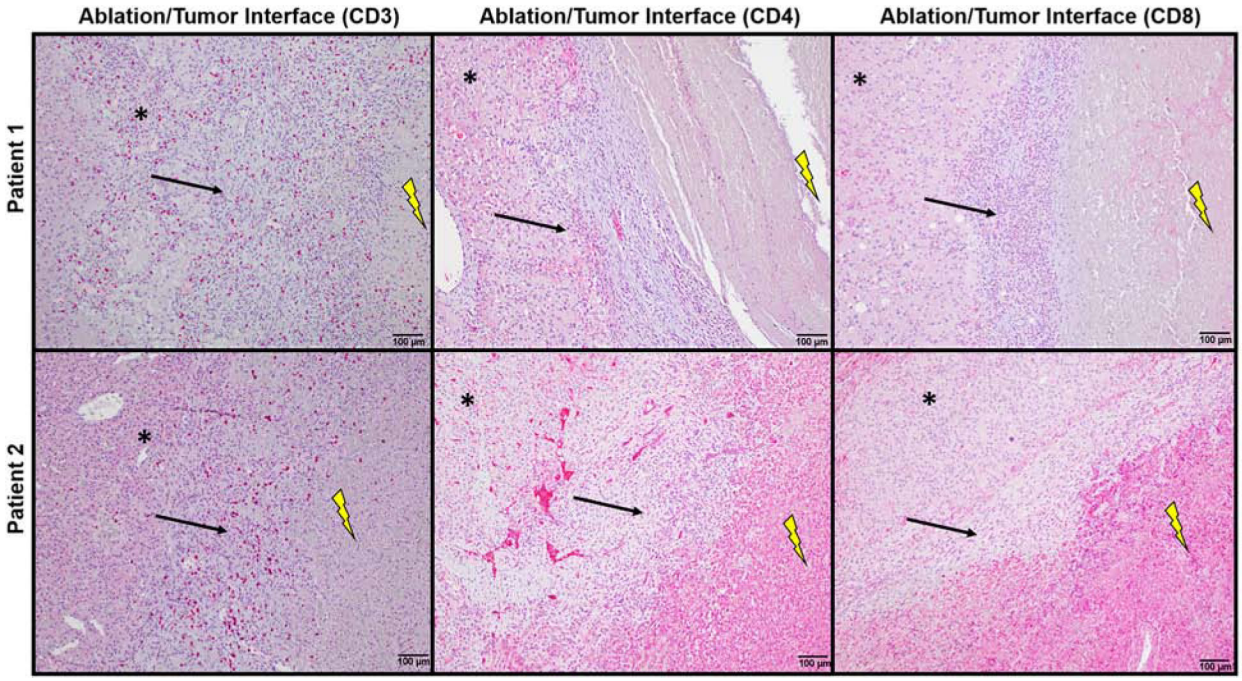

Figure 4.

Immunohistochemistry for CD3 (left), CD4 (center) and CD8 (right) on tumor samples from canine 1 (top) and canine 2 (bottom) showing infiltration of the ablation/tumor interface (arrows) with CD3+/CD4−/CD8− lymphocytes. Positively stained cells are red, however, positive staining in the ablation zone is due to cross-reaction with dead tissue rather than positive cells. Untreated HCC is denoted by (*) and the ablation zone by the bolt.

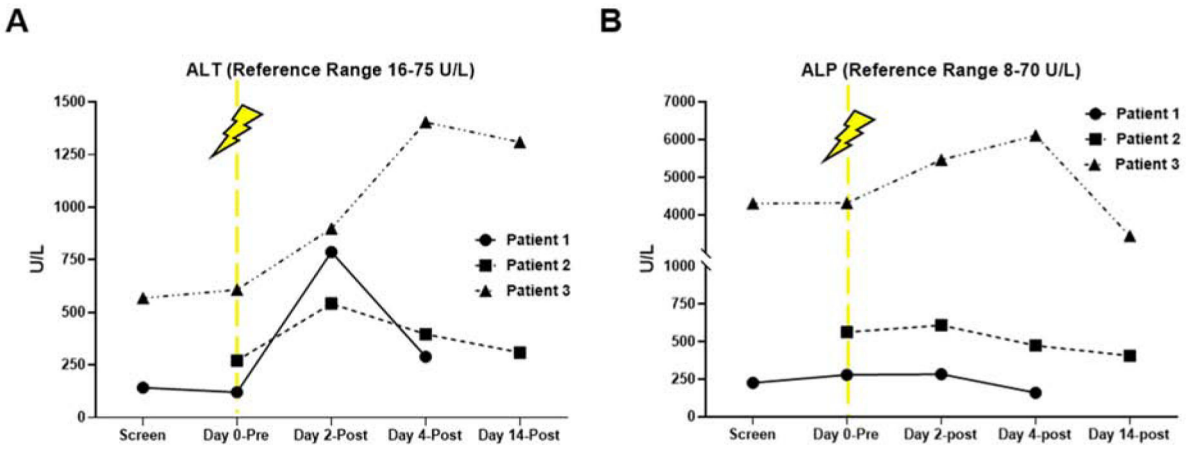

Figure 5.

(A) ALT and **(B)** ALP increased following HFIRE treatment (dashed line & bolt), but resolved over time following tumor removal (day 4).

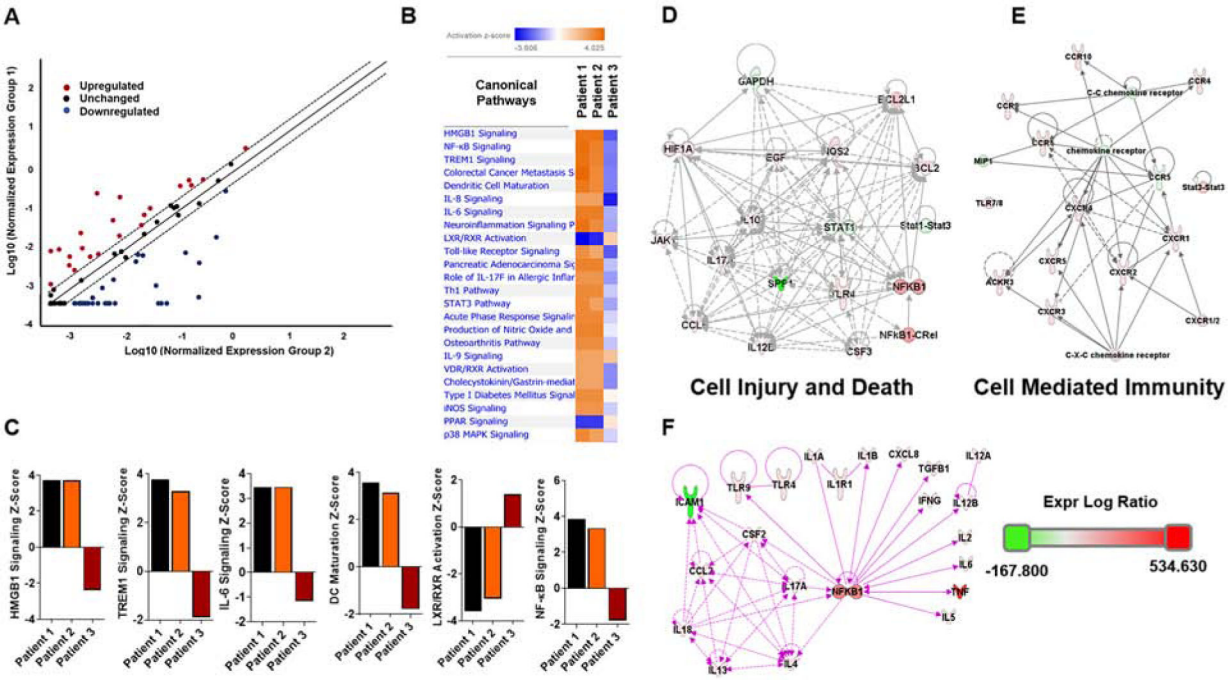

Figure 6.

(A) Scatter plot of gene expression array data illustrating the results from Table 1. Twenty-two gene expressions were significantly upregulated and twenty-nine were significantly downregulated following HFIRE treatment in all 3 canines compared to baseline. Change in expression of all other genes was less than 2-fold (unchanged) and represented by the solid black line. **(B)** IPA of global changes in gene expression patterns following HFIRE revealed diverse, but functionally related predications in canonical pathways significantly increased by HFIRE for canines 1 and 2. Conversely, the gene expression profile for canine 3 showed either no change or down-regulation of functionally similar canonical pathways. **(C)** The top six canonical pathways impacted by HFIRE, comparing pre-treatment to post-treatment, ranked by Z-score. Canines 1 and 2 are highly consistent, with canine 3 demonstrating opposing results. Pathways associated with the activation of cellular immunity and cell death are significantly upregulated following HFIRE treatment. **(D**, **E)** IPA network analysis identified two functional networks that fit the canonical pathways identified above, cell injury/death and cell mediated immunity. Both of these networks were significantly upregulated in all canines following HFIRE treatment. However, canine 3's data within the network was actually a significant downregulation moving towards lesser downregulation. **(F)** NF-κB signaling was one of the most dominate pathways impacted by HFIRE treatment. Gene expression patterns revealed a significant global up-regulation in NF-κB signaling.

Table 1.

Mean (n = 3) fold change in gene expression following HFIRE treatment compared to baseline. Only genes with significant changes in expression are shown, ranked from increased to decreased expression.

Gene name	Avg. ΔCt	ΔΔCt	Fold Change
SPP1	8.464517	0.002831	87.14
IL1R2	7.04305	0.007583	26.01
CCR5	11.26715	0.000406	20.51
IL18	9.43465	0.001445	16.56
TLR2	10.772517	0.000572	15.97
IL15	7.468417	0.005647	8.96
CSF1	10.111217	0.000904	6.63
CCL13	9.357183	0.001525	6.42
EGF	10.152517	0.000879	4.08
MYC	3.36785	0.096867	3.94
EGFR	5.224617	0.026744	3.84
ICAM1	2.849117	0.138781	3.84
CCL4	5.573083	0.021006	3.31
IFNG	11.26715	0.000406	2.9
IL13	7.092483	0.007327	2.77
PTGS2	8.85675	0.002157	2.77
TLR3	2.682717	0.155748	2.55
CCL20	9.81035	0.001114	2.42
FOXP3	8.36055	0.003042	2.28
LAMP1	1.988017	0.252085	2.19
MYD88	5.736417	0.018757	2.01
CCR2	5.956783	0.0161	−2.38
IL10	9.812583	0.001112	−2.91
CD244	9.75245	0.001159	−3.04
TGFB1	5.669317	0.01965	−3.05
CXCL8	6.082583	0.014756	−3.31
BCL2	9.523883	0.001358	−3.56
IGF1	9.51565	0.001366	−3.58
IL6	9.448917	0.001431	−3.75
PDCD1LG2	7.441417	0.005753	−3.76
CCR10	8.127617	0.003576	−3.78
IL23A	9.336483	0.001547	−4.05
IL1A	9.23725	0.001657	−4.34
GZMB	8.733317	0.00235	−4.45
CCR7	9.102383	0.001819	−4.76
CD274	8.996317	0.001958	−5.13
CXCR4	8.713083	0.002383	−6.24
TLR7	8.38755	0.002986	−7.82

Gene name	Avg. ΔCt	ΔΔCt	Fold Change
IL1R1	7.95095	0.004041	−10.58
IL5	7.800917	0.004484	−11.74
CCR1	7.69145	0.004838	−12.67
TNF	7.35655	0.006102	−15.98
JAK1	3.030883	0.122353	−16.31
APLNR	1.164283	0.446186	−23.79
BCL2L1	4.872617	0.034135	−31.5
HIF1A	2.21625	0.2152	−51.9
STAT3	4.721617	0.037901	−99.25
CCL2	4.523183	0.04349	−113.88
NFKB1	4.19035	0.054775	−143.43
CXCL10	2.251117	0.210061	−381.67